出國報告（出國類別：開會）

赴日本參加「第2 屆國際材料與智慧製造研討會(ICMIM 2018)」出國報告

服務機關：核能研究所
姓名職稱：林泰男 副工程師
派赴國家/地區：日本
出國期間：**107** 年 **8** 月 **22** 日~**107** 年 **8** 月 **26** 日
報告日期：**107** 年 **10** 月 **11** 日

摘　要

核能研究所核子燃料及材料組林泰男聘用副工程師，奉派於 107 年 8 月 22 日至 26 日，赴日本北海道札幌市(Sapporo, Hokkaido Japan)，參加第 2 屆國際材料與智慧製造研討會(ICMIM 2018)。林員於本屆會議中就本所於固態氧化物燃料電池(Solid oxide fuel cell, SOFC)領域研發成果進行英語論文口頭報告，題目為「Investigation on the performance and durability behavior for the anode-supported solid oxide fuel cell with composite cathodes」。本次前往日本札幌市參加 ICMIM 2018 國際研討會，以 SOFC-MEA 研發成果進行學術論文口頭發表，藉由此會議交流與國際上相關產學研專家學者討論燃料電池技術研發現況並建立研發資訊交流管道。另外透過九州大學石原達己教授協助聯繫，此次亦前往北海道大學拜訪秋山友宏(Tomohiro Akiyama)教授，針對粉末合成技術研發進行交流討論。

新材料技術是當今高科技革命的重要標誌之一，大多數高科技發展都是在新材料技術突破的前提下進行的。材料開發與研究是戰略性新興產業的基礎，在高科技產業應用扮演著極重要作用，是推動技術進步的動力。每一項重大技術開發和新產品的成功開發都離不開新材料的發現和應用。為了使新材料得到實際應用，必須仰賴製程技術的精進。毫無疑問，製造業在各行各業都至關重要。隨著資訊、通信和網絡技術的快速發展，傳統工業製造與製程朝向智慧生產方向演進，並且使得工業產品與流程達到智慧化準確畫與高效率的商業規格。本所於 SOFC 之研發成效顯著受到國際肯定，並積極參與國際上 SOFC 相關研討會。

本次大會主要為各工程材料製造領域的研討會，除了主要聚焦在材料與製造，投稿論文主題不限於筆者專業領域 SOFC，而是廣度較大的工程製造領域的知識意見交流，舉凡材料合成、製程改良、精密製造與人因工程等學術論文研究方向皆有所報導。本所在 SOFC 之發展秉持 from powder to power 的研發主軸，唯目前已匯集了各方面整合型的研發成果並朝向技術產業化持續推動，除了材料研發之外，製造技術的強化與提升系統產品產業應用可行性時為重要議題。本次會議為材料與製造相關，建議本所相關研發除持續精進 SOFC 技術之外，亦值得

投入資源於終端產品實務應用的推廣。

目　次

頁次

摘　要 i

一、目的 1

二、過程 2

三、心得 12

四、建議事項 23

五、附錄 25

附錄(一) 林員投稿論文摘要、接受函及邀請函 25

圖目錄

頁次

圖 1 札幌地理位置與札幌站 ..... **錯誤! 尚未定義書籤。**

圖 2 中華航空 CI 130 航班。 ..... **錯誤! 尚未定義書籤。**

圖 3 北海道大學與秋山友宏教授團隊。 4

圖 4 ICMIM2018 舉辦地點 Hotel Mystays Premier Sapporo Park 及與會人員合影。…….. 4

圖 5 議程表。…….9

圖 6 本所論文發表證明與最佳口頭報告獎狀。……...11

圖 7 Si_3N_4 與 AlN 的相關特性。 13

圖 8 Si_3N_4 與 AlN 的合成與分析。……..13

圖 9 螢光粉與合成方式。……14

圖 10 以燃燒合成法製備之螢光粉與商購產品特性。……..15

圖 11 From lab-scale to Industrial available batch-scale。……15

圖 12 退火 ZnO 薄膜表面形貌與光穿透特性分析。……17

圖 13 PVA 以及 Pd-TiO2 / PVA 奈米複合薄膜光特性分析。**錯誤! 尚未定義書籤。**8

圖 14 PVA-PVP / SnO2 奈米複合薄膜表面形貌分析。..**錯誤! 尚未定義書籤。**9

圖 15 LMO 薄膜 XRD 與表面形貌分析。 20

圖 16 陽極支撐質子傳輸型燃料電池為結構與效能。 21

圖 17 低溫型燃料電池開發之微結構。 22

一、目的

本所於 SOFC 之研發始於 2003 年，在陽極支撐型固態氧化物燃料電池的研發領域秉持著從「粉末到功率 (From powder to power)」的概念，持續進行技術深耕與產品開發，近年來研發成效顯著受到國際肯定，並積極參與國際上 SOFC 相關研討會；本次林泰男博士奉派代表本所 SOFC 計畫前往日本札幌市參加第 2 屆國際材料與智慧製造研討會(ICMIM 2018)國際研討會，以 SOFC-MEA 研發成果進行學術論文口頭發表，藉由此會議中氫能與燃料電池議題與國際上相關產學研專家學者討論燃料電池技術研發現況並建立研發資訊交流管道，以吸收國際上最新的 SOFC 發展資訊，藉此提升本所技術研發能量。本所 SOFC 相關研發工作成果計投稿本屆口頭發表會議論文 1 篇，已獲接受並排定於會議進行論文發表。藉由參加本屆國際會議，可以掌握日本/國際最新之相關各個領域研發現況及發展趨勢，並尋求可能之技術推廣及強化國際合作關係與提昇本所之研發量能。林員奉派參加本屆大會，投稿之會議論文題名為：「Investigation on the Performance and Durability Behavior for the Anode-supported Solid Oxide Fuel Cell with Composite Cathodes」。

二、過程

核能研究所林泰男副工程師，奉派於 107 年 8 月 22 日至 26 日，赴日本札幌參加「第 2 屆國際材料與智慧製造研討會(ICMIM 2018)國際研討會」。本項國際材料與智慧製造研討會(ICMIM)是 2017 年 8 月 21 日至 23 日於新加坡國立大學首次舉行，聚焦在材料與智慧製造領域的專家討論與分享，今年則為第 2 屆；本屆會議於日本札幌市(Sapporo, Japan)舉行，札幌位於日本北海道(Hokkaido)，為日本第 5 大城市(如圖 1)。除了有豐富資源與多樣季節景色，其在教育研究方面北海道大學為知名大學，在日本以及世界上均佔有重要的學術地位。林員本次前往日本參加會議之交通，採搭乘本國籍航空直達北海道新千歲機場之航班，再轉乘地鐵進入札幌市並參加會議與論文發表演講。

圖 1. 札幌地理位置(https://zh.wikipedia.org/wiki/%E6%9C%AD%E5%B9%8C%E5%B8%82)與札幌站

本次參加國際會議準備過程及與會行程簡述如下:

- 107/03/22　依計畫需求檢索本年度於日本舉辦之相關能源領域國際研討會
- 107/03/31　決定參加 ICMIM2018 / 辦理出國計畫變更作業 / 準備投稿論文
- 107/05/24　完成全文投稿

- 107/06/19　辦理出國簽呈所內簽核程序
- 107/06/29　所內出國公差申請核准
- 107/08/22　搭乘中華航空 CI 130 由桃園國際機場出發 (圖 2)。
- 107/08/22　抵達新千歲機場。搭 JR 抵達札幌市區。
- 107/08/23　前往北海道大學進行簡要拜會參訪。
- 107/08/24 ~ 107/08/25
  參加 ICMIM2018 國際會議與論文發表演講。
- 107/08/26　搭乘搭乘中華航空 CI 131 由新千歲機場回台。

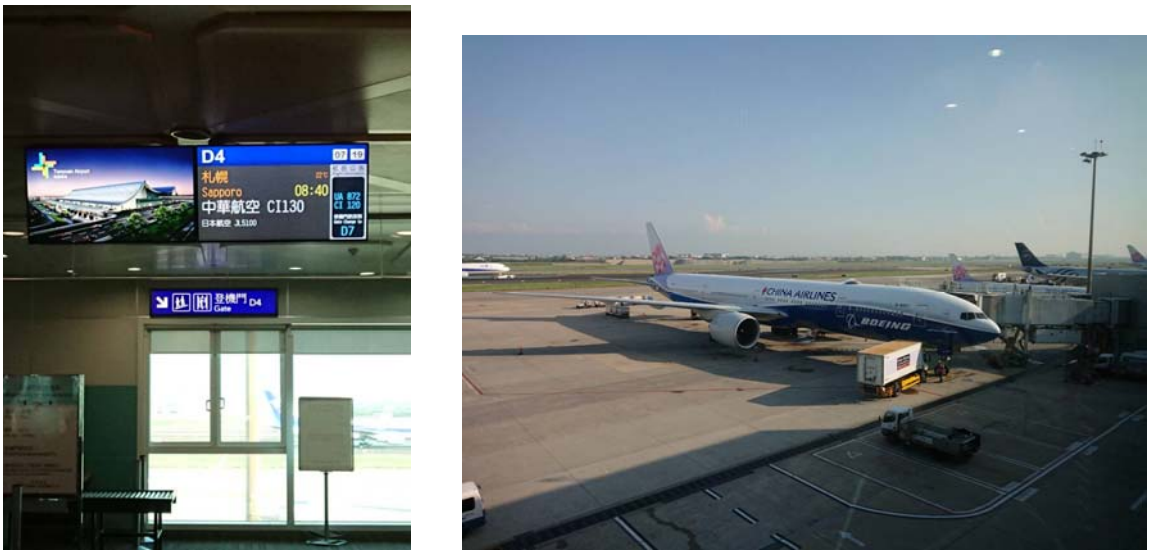

圖 2. 中華航空 CI 130 航班

公差工作內容說明如下:

（一） 參加會議：

核能研究所林員於 8 月 23 日前往北海道大學拜訪秋山友宏(Tomohiro Akiyama)教授 (圖 3)，針對粉末合成技術研發進行交流討論，秋山實驗室長期研究燃燒合成法(Combustion Synthesis)與氧化物、氮化物等粉末研製與應用的領域並素有聲譽；此次是透過與本所關係良好並簽有 SOFC-MEA 研發合作備忘錄之九州大學石原達已教授協助聯繫成行。筆者由下榻飯店

沿地鐵向北步行至北海道大學約 30 分鐘。

林員於 2018 年 8 月 24 日至 26 日全程參加「第 2 屆國際材料與智慧製造研討會(ICMIM 2018)國際研討會」，本屆會議札幌市中心之 HOTEL MYSTAYS PREMIER Sapporo Par 舉行(如圖 4)舉行，並同時於會場進行海報論文

圖 3. 北海道大學與秋山友宏教授團隊 (經秋山教授同意合影)

圖 4. ICMIM2018 舉辦地點 Hotel Mystays Premier Sapporo Park(http://www.icmim.org/)及與會人員合影

發表。本屆會議最終定案議程(Session)計有 5 個不同材料製造應用領域 (圖 5)，包括：

Session 1：Mechanical and Manufacturing Engineering (10 presentations)

- Increasing the Dimensional Accuracy of U-bend Product of High Strength Steel Sheets by Pressure Pad (***Pongsakorn Leetrakul***)
- Increasing the Hole Expansion Ability of High Strength Steel Sheet by Improving the Pre-Hole Shearing Process (***Prasan Saengkhiao***)
- An Improved Gravitational Coefficient Function for Enhancing Gravitational Search Algorithm's Performance (***Pattarawet Tharawetcharak***)
- An Approach to Plan the Spray Path (***Yongxiong Zhang***)
- Remaining Useful Life Prediction of Cutting Tools Based on Support Vector Regression (***Yingchao Liu***)
- A Calculation Method for Dressing Amount of Monolayer Electroplated Grinding Wheel Based on Zernike Moment ***(Bin Li)***
- Quality Assurance of Injection Molding Quality by Monitoring and Diagnosis of Mold and Machine (***Ming-Shyan Huang)***
- Development of Strategic Supply Chain Management for Autoparts and Components Manufacturing Company (***Nuttawut Rojniruttikul)***
- Universal Design Research Applies to New Products with Unclear Design Factors (***Wei Miao)***
- The Effects of Robot Voice Style on the Perceived Robot Personalities in Different Occupational Fields ***(Xiao Dou)***
- Modeling and Characterization of Lathe Spindle Cutting Patterns with Crossed Roller Bearing Installed ***(Xiaozhong Song)***

Session 2 : Material Physics and Material Mechanics (9 presentations)

- Low Temperature Liquid Phase Growth and Characterizations of 2D Crystalline Inse İmplemented with Temperature Difference Method under Controlled Vapor Pressure (***Chao Tang)***
- Low Temperature Liquid Phase Growth of Ge Doped Gase and GaSe1-xTex Crystal for Highly Efficient Thz Light Source ***(Yohei Sato)***
- Solvent Engineering for Enhanced Cubic Phase CsPbI3in Perovskite Solar Cells ***(Ting Zhang)***
- Epitaxial Growth of Well-Aligned Single-Crystalline VO2 Micro/Nanowires Assisted by Substrate Facet Confinement ***(Liangxin Wang)***
- Strong Hole Self-Doping in LaMnO3Thin Film on a-SiO2Substrate produced by Metal Organic Decomposition Method (***Hiromi Kobori)***
- High Photocatalytic Activity of Amorphous TiO2Nanotube Arrays and Relevant Mechanism ***(Liang Hao)***
- Preparation of Concomitant Schottky Junction and Cocatalyst Compound: Ni(OH)2/Pt/TiO2 and Its Enhanced Photocatalytic Performance (***Xiaochen Ren)***
- The 3-D Finite Element Analysis on Elastic-Plastic Micromechanical Response of the Particle Volume Fraction (***Yong-Ming Guo***)
- Predicting Crystal Structures of Materials with İnterfaces: A Study on Grain Boundaries of a Complex Oxide (***Wei LiCheah)***

Session 3 : Functional Materials and Devices (9 presentations)

- Investigation of Mechanical and Electrical Characteristics of Flexible Conductive Polymer Substrates for Whole-folding Test ***(Bor-Jiunn Wen)***
- Influence of Anneal Temperature in Air on Surface Morphology and Photoluminescence of ZnO Thin Films ***(Sujun Guan)***
- Intelligent Manufacturing of Highly (111)-Preferred Nanotwinned Cu Films and Their Applications in Cu-to-Cu Direct Bonding ***(Chih Chen)***

- Applying the Friction-induced Method to Graphene Fabrication ***(Mingxi Chen)***
- Conductive Textiles for Electrothermal Heating and Actuation ***(Dharshika Kongahage)***
- Gel-like Graphene Composite with Self-Healing and Reshaping Properties Inspired by Bio-Mineralization ***(Shuyuan Lin)***
- Electromagnetic Wave Absorption Performance of ZnO@ZnS Nanotube by Waper gas-phase Synthesis (***Mengxiao Sun)***
- Fabrication and Mechanical Property Evaluation of ASD Occluders Made from Shape Memory Alloys (***Thepphithak Rueangmontree)***
- Classification of Agricultural Questions Based on Rule Templates and Svm ***(Peng Zhu)***

Session 4 : Biomedical Materials and Biomedical Engineering (8 presentations)

- Plasmonic Nanoshells BasedMetabolite Detection for In-vitro Metabolic Diagnostics and Therapeutic Evaluation (***Lin Huang)***
- Investigation of Colloidal Behavior of Surface-Modified Superparamagnetic Iron Oxide Nanoparticle under Biological Environment (***Wid Mekseriwattana)***
- Focused Ion Beam Modification of Hexagonal Boron Nitride ***(Erik Roede)***
- Highly Emissive Dye-Sensitized Upconversion Nanostructure for Dual-Photosensitizer Photodynamic Therapy and Bioimaging ***(Jiating Xu)***
- Glutathione Mediated Size-Tunable UCNPs-Pt(IV)-ZnFe2O4Nanocomposite for Multiple Bioimaging Guided Synergetic Therapy (***Huiting Bi****and)*
- Improving Breast Cancer Cell Targeting Using Riboflavin Conjugated Poly(Lactic-Co-Glycolic Acid) Nanoparticles (***Komkrich Sawasdee****)*
- Development of Theranostic Polymeric Nanoparticles for Breast Cancer Detection and Treatment (***Supreeya Srisuk****)*
- Mıcromechanıstıcally Modulated Cardıomyocyte Alıgnment In Vıtro (***Carina J.***

Lee)

Session 5 : Electrochemistry and Chemical Engineering (8 presentations)

筆者口頭報告議程排定為本場次議程(25日下午)。

- Highly Efficient Solar Vapor Generation via Bioinspired Capillary-Driven Pump ***(Haifeng Jiang)***
- High Efficiency and Low Hysteresis Solar Cells Based on Perovskite with Triple Cation and Mixed Pb-Sn (***Long Ji)***
- Synthesis and Characterization of Highly Porous LaCoO3 Catalyst prepared by Nanocasting for ORR and OER for Secondary Zinc-Air Batteries (***Byungho Song)***
- Investigation on the Performance and Durability Behavior for the Anode-Supported Solid Oxide Fuel Cell with Composite Cathodes (***Tai-Nan Lin)***
- Effects of Cation-Mixed Grain Boundary on the Electrochemical Performance of Ni-Rich Cathode Material for Lithium Ion Batteries (***Sanghun Lee)***
- Graphene Oxide/Polyacrylonitrile Air Filters for EffectiveCapture of PM2.5and Ultrafine Particleswith a Low Filtration Resistance (***Jing Li)***
- Synthesis of Advanced Hybird Polymer Nanocomposite Material(TiO2-SiO2) by Mechanical Stirring Technique (***Adel K. Mahmoud)***
- Synthesis, Characterization and Its Photocatalytic of Copper Oxide (CuO) Powder (***Pusit Pookmanee)***

Brief Schedule for Conference

Day 1	**August 24, 2018 (Friday)** 10:00~17:15 **Venue:** ***Lilas S (2st floor)*** Arrival Registration, Keynote Speech and Conference Presentations
	Venue: ***Lobby*** **Arrival Registration** 10:00~12:00
	Afternoon Conference
	Venue: ***Lilas S (2st floor)*** **Opening Remark** 13:00~13:05 Prof. Masayoshi Tonouchi, Osaka University, Japan **Keynote Speech I** 13:05~13:40 Assoc. Prof. Pan Jisheng, National University of Singapore, Singapore **Keynote Speech II** 13:40~14:15 Prof. Masayoshi Tonouchi, Osaka University, Japan
	Session 1 (part 1): 14:15~15:30 **Venue:** ***Lilas S (2st floor)*** 5 presentations-Topic: "Mechanical and Manufacturing Engineering"
	Coffee Break & Group Photo Taking 15:30~15:45
	Session 1 (part 2): 15:45~17:15 **Venue:** ***Lilas S* (2st floor)** 6 presentations-Topic: "Mechanical and Manufacturing Engineering"
Day 2	**August 25, 2018 (Saturday)** 9:00~18:00 **Venue:** ***Lilas & Lilas S (2st floor) & Lilas N (2st floor)*** Arrival Registration, Keynote Speech and Conference Presentations
	Morning Conference
	Venue: ***Lilas (2st floor)*** **Opening Remark** 9:00~9:05 Prof. Takashige Omatsu, Chiba University, Japan **Keynote Speech I** 9:05~9:40 Prof. Shen-Ming Chen, National Taipei University of Technology, Taiwan **Keynote Speech II** 9:40~10:15 Prof. Der-Jang Liaw, National Taiwan University of Science and Technology, Taiwan **Coffee Break & Group Photo Taking** 10:15~10:35 **Keynote Speech III** 10:35~11:10 Prof. Hongwei Zhu, Tsinghua University, China **Keynote Speech IV** 11:10~11:45 Prof. Jun Ding, National University of Singapore, Singapore **Keynote Speech V** 11:45~12:20 Prof. Takashige Omatsu, Chiba University, Japan
	Lunch: 12:20~13:30 **Venue:** ***Terra (1st floor)***

圖 5 (a). 議程表

2018 SAPPORO CONFERENCE

	Afternoon Conference	
	Session 2: 13:30~15:45 **Venue:** ***Lilas S (2st floor)*** 9 presentations-Topic: "Material Physics and Material Mechanics"	**Session 3:** 13:30~15:45 **Venue:** ***Lilas N (2st floor)*** 9 presentations-Topic: "Functional Materials and Devices"
	Coffee Break:	15:45~16:00
	Session 4: 16:00~18:00 **Venue:** ***Lilas S (2st floor)*** 8 presentations-Topic: "Biomedical Materials and Biomedical Engineering"	**Session 5:** 16:00~18:00 **Venue:** ***Lilas N (2st floor)*** 8 presentations-Topic: "Electrochemistry and Chemical Engineering"
	Poster Session 9:00~18:00	**Venue:** ***Lilas (2st floor)***
	Dinner: 19:00	**Venue: Terra** ***(1st floor)***
Day 3	**August 26, 2018 (Sunday)** 8:30~17:00	One-day Academic Visit

Tip: Please arrive at the Conference Room 10 minutes before the session begins, and upload PPT/ PDF file into the conference laptop.

圖 5 (b). 議程表

另外每日議程進行前皆有 Keynote speech，由大會邀請之各國專家學者進行邀請演講，講員包含新加坡國立大學(National University of Singapore) Professor Jishen Pan、日本大阪大學(Osaka Universiaty) Professor Masayoushi Tonouchi、台北科技大學陳生明教授、台灣科技大學廖德章教授、中國北京清華大學 Professor Hongwei Zhu、新加坡國立大學(National University of Singapore) Professor Jun Ding 以及日本千葉大學(Chiba University) Professor Takashige Omatsu 等人；演講內容包含材料、製造、特性分析與實務應用。

林員參加本屆會議，並於 8 月 25 日下午於 Session 5: Electrochemistry and Chemical Engineering 發表英語口頭論文 1 篇：「Investigation on the performance and durability behavior for the anode-supported solid oxide fuel cell with composite cathodes；Tai-Nan Lin, Yang-Chuang Chang, Maw-Chwain Lee, Wei-Xin Kao」，本篇論文獲得 Electrochemistry and Chemical Engineering Session: Best Oral Presentation Paper (圖 6)。本項議程主持人為

國立交通大學材料系陳智教授。

Participation and Presentation Certificate

for

2018 2nd International Conference on Materials and Intelligent Manufacturing (ICMIM 2018)

Sapporo, Japan August 24-26, 2018

Paper title: Investigation on the Performance and Durability Behavior for the Anode-Supported Solid Oxide Fuel Cell with Composite Cathodes

Presenter's name: Tai-Nan Lin (Z2002)

Presenter's affiliation: Institute of Nuclear Energy Research, Taiwan

trans tech publications inc. Publishers in Sedence and Engineering

Conference Chair

Organization

CERTIFICATE

This is to certify that

Tai-Nan Lin

from

Institute of Nuclear Energy Research, Taiwan

has attended, and delivered an oral presentation in 2018 2nd International Conference on Materials and Intelligent Manufacturing (ICMIM 2018) in Sapporo, Japan during August 24-26, 2018. His/her presentation has been selected as one of the best oral presentations.

Conference Chair

ICMIM 2018

BEST

圖 6. 本所論文發表證明與最佳口頭報告獎狀

（二） 回程：

本項會議於 8 月 25 日下午結束，26 日則為大會安排參訪行程；由於此次公差任務已順利完成，因此林員並無參加大會參訪，於 8 月 26 日返台，回程路線由札幌站搭地鐵前往新千歲機場，爾後搭乘中華航空 CI-131 航班直飛返回台灣桃園國際機場。

三、心得

（一） 本文作者林員本次赴日本北海道札幌市參加 2 屆國際材料與智慧製造研討會 ICMIM2018 國際會議並順利完成口頭英語論文發表與全文投稿。本次大會延續 2017 年於新加坡舉行之 ICMIM2017 會議，包括 5 項聚焦議程，共計收到 44 篇論文摘要投稿，14 篇海報論文，並邀請各國專家學者進行多元化的 Keynote 演講。本項會議主要聚焦在材料與製造，投稿論文主題不限於筆者專業領域 SOFC，而是廣度較大的工程製造領域的知識意見交流：相信藉由參與本屆會議與發表論文，對於促進國際學術交流與展現研發成果，以及提升技術水準與對於研究計畫的持續進行，均能產生正向效益。

（二） 本所 SOFC-MEA 技術積極推廣產業應用與技術授權，研發除了在量產技術建立與產品開發之外，持續提升發電效能與降低操作溫度為未來研發重點。本次原擬透過九州大學石原達己教授協助聯繫(2018.03.31)，計畫前往北海道大學應用化學系所拜訪幅崎浩樹(Hiroki Habazaki)教授，針對質子傳輸型(Proton-conducting) SOFC 的研發進行交流討論。唯在投稿完成後向幅崎教授確認拜訪行程之時，於 6 月 30 日幅崎教授臨時表示屆時有重要會議無法接待本所參訪討論。因此改為請石原教授協助聯絡並感謝秋山友宏教授同意本所人員前往進行簡要拜訪討論。秋山教授主持的「Energy Conversion Materials group」長期研究燃燒合成法研製氧化物、氮化物、氟化物等粉末材料，並研究應用與量產推廣。以燃燒合成法研製氮化物為例作說明，氮化矽與氮化鋁皆擁有優異的機械、化學與電性特性 (如圖 7 / 圖 8)。在燃燒反應開始時依需求分別添加助反應的 NaCl 與 NH_4Cl 於反應物中，可有效降低燃燒熱並幫助合成反應進行而得較佳性質的終端產物粉體。另一實例則是針對 YAG : Ce 螢光粉的合成。LED 螢光粉(Phosphor)的發

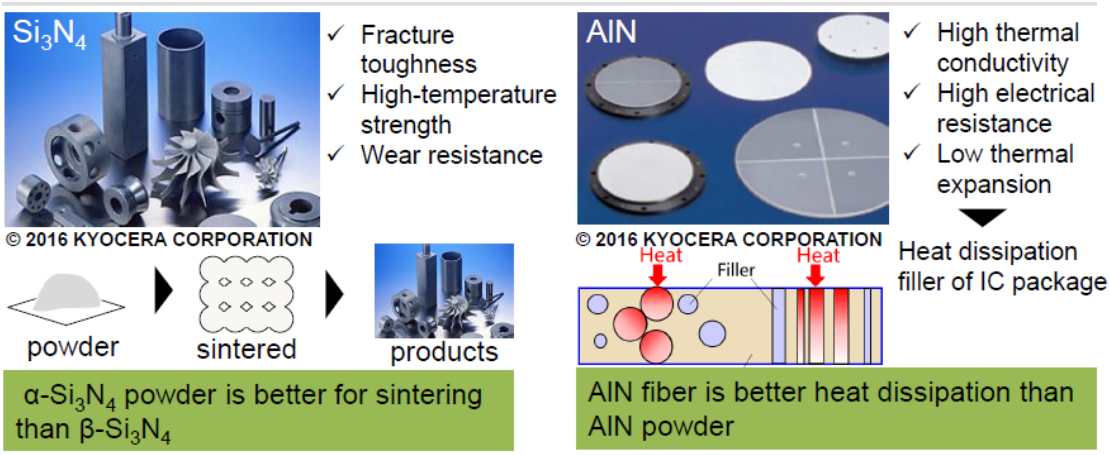

圖 7. Si_3N_4 與 AlN 的相關特性 (Prof. T. Akiyama: http://anergy.caret.hokudai.ac.jp/member_0_e.html)

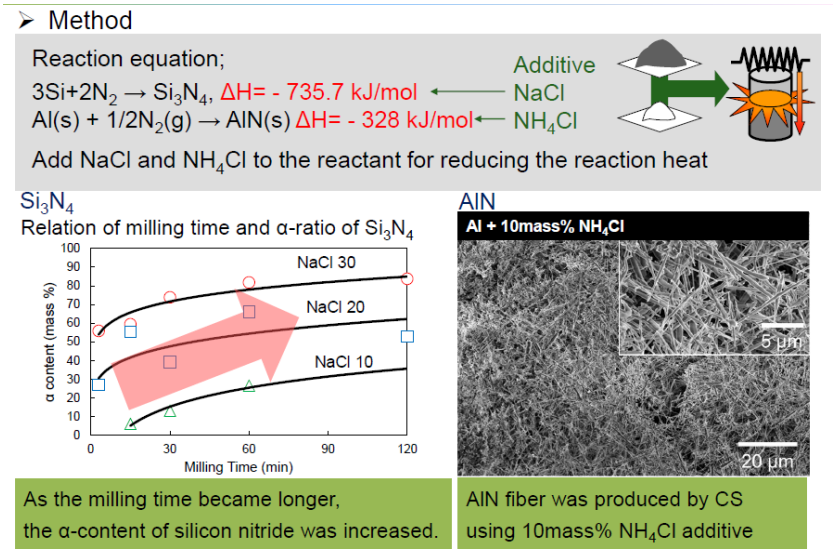

圖 8. Si_3N_4 與 AlN 的合成與分析 (Prof. T. Akiyama: http://anergy.caret.hokudai.ac.jp/member_0_e.html)

展可從 1996 年日亞化學（Nichia）所開發的白光 LED 開始，Nichia 使用的方式是 Blue LED(InGaN)晶片＋YAG 螢光粉(Y3Al5O12:Ce；釔鋁石榴石)，這也是到目前為止公認效率最高方式。YAG 螢光粉是一種陶瓷粉末，螢光物質受光刺激後，內部電子受激到高能階的激發狀態後，回到原有的低能階狀態時，將能量以光的形式輻射出來，而不同螢光陶瓷粉

末受光激發後發出的光顏色也會一樣。傳統上合成以固態反應法進行，合成條件須在 1500 °C 高溫還原氣氛下進行多次反應，耗費時間與大量能耗；秋山實驗室以燃燒合成法氧化鋁加入鋁與氧氣，自發燃燒反應溫度達 1500 °C 以上，優點是節省能耗並縮短製程時間與成本；且終端產物粉體螢光發光效率與商購螢光粉接近 (圖 9 / 圖 10)。秋山實驗室從學術研發到量產應用的技術能量如圖 11 所示，如同本所研發 SOFC 的主軸精神一樣 From powder to power，學術的基礎研究需要在產業實現才能彰顯其技術價值。

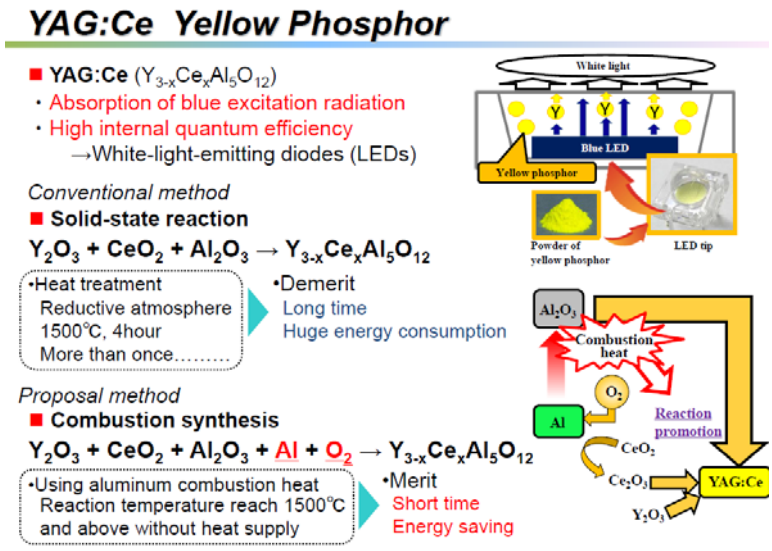

圖 9. 螢光粉與合成方式 (Prof. T. Akiyama: http://anergy.caret.hokudai.ac.jp/member_0_e.html)

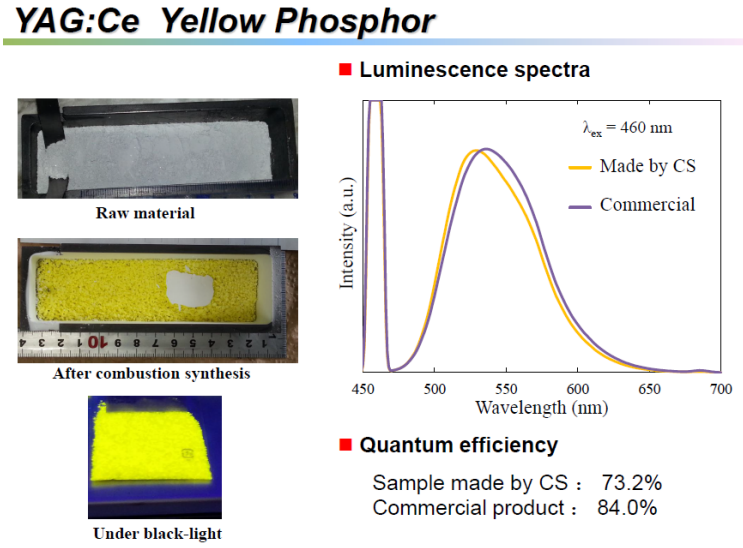

圖 10. 以燃燒合成法製備之螢光粉與商購產品特性 (Prof. T. Akiyama: http://anergy.caret.hokudai.ac.jp/member_0_e.html)

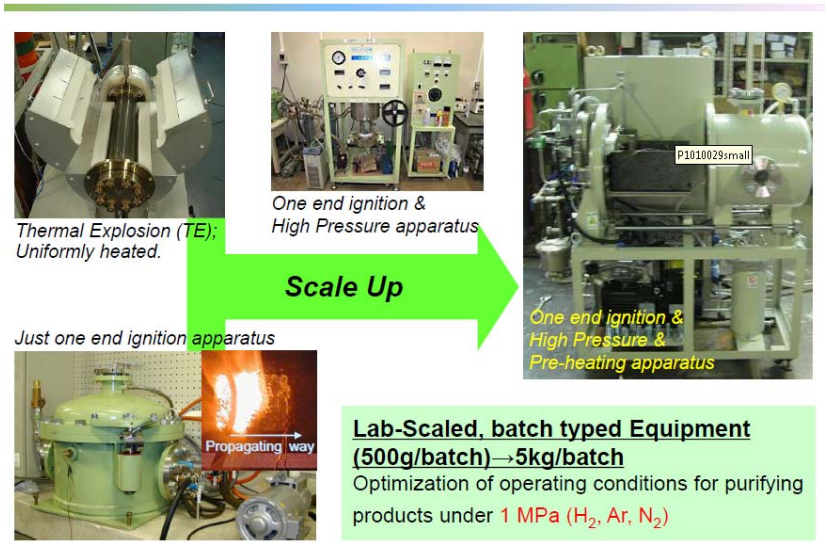

圖 11. From lab-scale to Industrial available batch-scale (Prof. T. Akiyama: http://anergy.caret.hokudai.ac.jp/member_0_e.html)

（三） 本次開會聯繫感謝日本九州大學石原達己教授(應用化學系教授兼任 WPI 計畫之 I2CNER 國際頂尖研究中心(International Institute of Carbon

Neutral Energy Research)副執行長)協助，其研究專長為高溫燃料電池、陶瓷材料、能源轉換與光觸媒等領域。針對筆者執行之 SOFC 計畫相關的資訊以下簡要列出。日本在 SOFC 的耐久評估 NEDO 的 degradation project 之目標為每千小時衰退率在 0.2 %以下 (end of 2018)，基於計畫與場域的試驗因素，持續的投資與驗證工作仍將進行；特別是在產業應用到了一定的時間， SOFC 系統應用之成本降低議題(decrease of cost)是影響產業發展至關重要的關鍵。Kyocera 低溫型之 compact Flat-Tube (tube thickness ~ 2 or 3 mm)結構之 700W 系統的開發應用，並計畫朝向 3~5 kW 的系統開發進行實務驗證。另外日本 NGK/NTK 公司亦開發 planar type SOFC 並有相當成效，module efficiency 大於 60 %，惟 degradation rate 每千小時介於 0.4 %。本所 SOFC-MEA group 原規劃與石原教授實驗室合作進製作 double columnar structure 的陰極結構以提昇陰極端 oxygen dissociation characteristic 反應特性而提升發電效能，擬針對較小元件尺寸電池進行研製開發，本次開會期間亦與石原教授進行 email 與電聯討論，並期望在未來能持續維持彼此合作關係對本所 SOFC-MEA 的研發提供助益。

（四） 本次大會主要為各工程材料製造領域的研討會，並不單單聚焦於筆者從事之固態氧化物燃料電池研究，以下提出幾項其他研究領域的簡要心得。東京理科大學發表之論文「Influence of anneal temperature in air on surface morphology and photoluminescence of ZnO thin films」，成功利用射頻磁控濺射法在石英基板上製作氧化鋅薄膜，並在空氣環境中進行退火與研究退火溫度對晶體的結構、表面形貌、光學性質之影響調查。研製之 ZnO 薄膜顯示為纖鋅礦 ZnO 晶體結構。隨著退火溫度的升高，(002) ZnO 薄膜的晶面成長且晶粒移動規模增加。退火溫度對薄膜表面形貌影響明顯，溫度提高薄膜表面呈顆粒狀結構成長，部分則結合成較大晶粒。

退火 ZnO 薄膜的透過率明顯在沒有的情況下，該區域從 400nm 增加到 500nm 影響帶隙。退火溫度的影響 ZnO 薄膜的光致發光特性明顯，特別是在可見光範圍內。由 XPS 結果證實退火溫度為在 350 °C 時 ZnO 薄膜顯示出最高的光激發螢光頻譜，原因為氧空位的相對濃度有所提升。

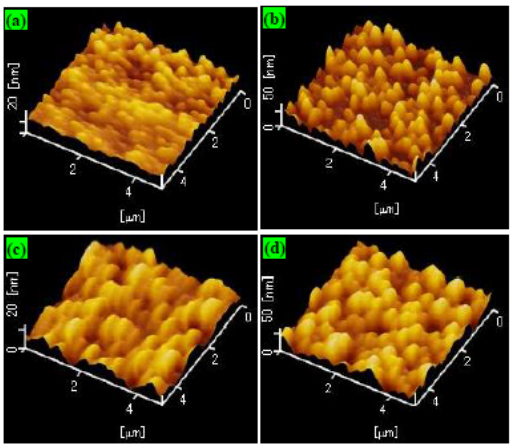

Fig. 2. Surface morphology of the samples. (a) ZnO, (b) Air-350, (c) Air-380, (d) Air-400.

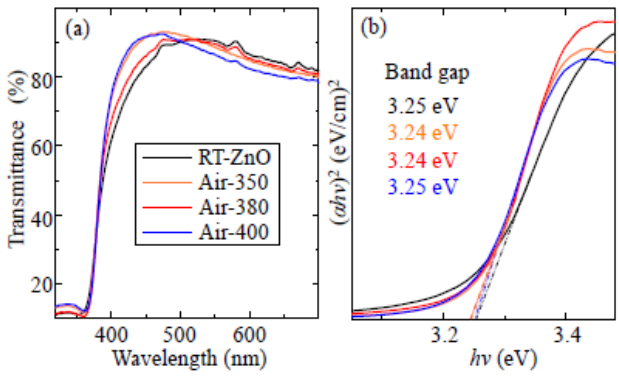

Fig. 3. (a) Optical transmittance spectra and (b) plots of $(\alpha h\nu)^2$ against $h\nu$ of the samples.

圖 12. 退火 ZnO 薄膜表面形貌與光穿透特性分析 (From Sapporo Conference -ICMIM 2018 Abstract book)

（五） 印度 Mangalore University 發表之論文：「Surface, Temperature and Optical Properties Pd-TiO_2 doped PVA Nanocomposite」，使用溶液流延技術製備純 PVA 以及 Pd-TiO_2 / PVA 奈米複合薄膜，並探討 Pd-TiO_2 奈米粒子摻雜對 PVA 之結構、光學和熱性能的影響。 FTIR 研究證實了 Pd-TiO_2 奈米顆粒與 PVA 聚合物的 OH 基相互作用並形成複合產物，影響複合材料的光學和熱學性質。從這些研究中得知摻雜的 Pd-TiO2 納米粒子對其有很大的影響聚合物奈米複合物的形態，熱學和光學性質。奈米粒子摻雜量會增加 OH 鍵結而強化 charge transfer complex {= CTC} - 電荷轉移錯合物的形成。

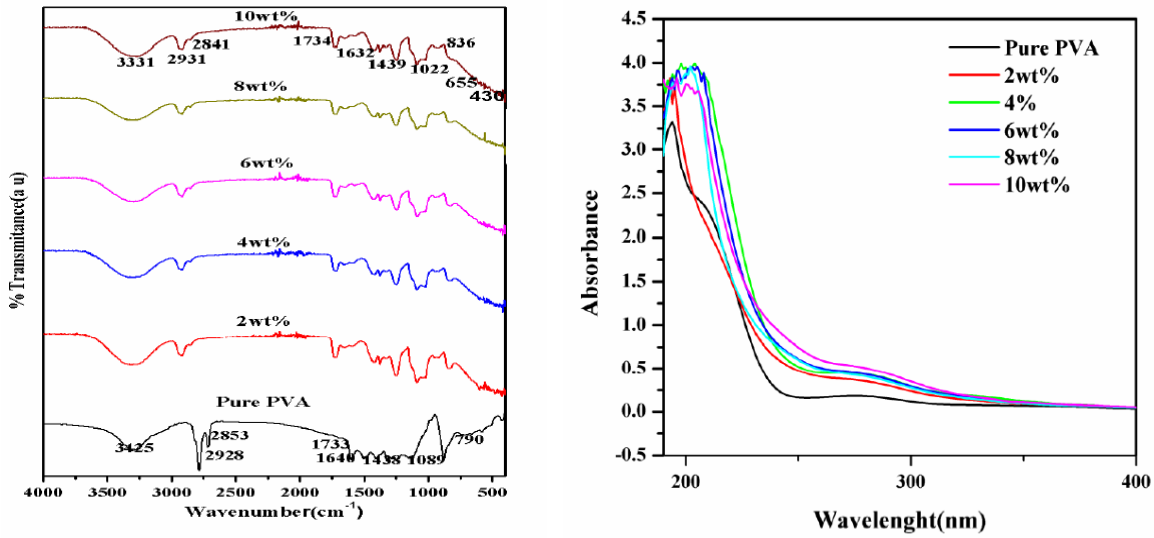

圖 13. PVA 以及 Pd-TiO_2 / PVA 奈米複合薄膜光特性分析 (From Sapporo Conference -ICMIM 2018 Abstract book)

(六) 印度 Mangalore University 發表之論文：「Effect of SnO_2 Nanoparticle doping on Structural, Morphological and thermal properties of PVA-PVP polymer blend」，合成 n 型半導體 SnO_2 奈米顆粒，研究奈米粒子摻雜對 PVA-PVP 聚合複合物的結構、形態和熱性質的影響。純和 PVA-PVP / SnO_2 奈米複合薄膜是使用溶液流延技術製備。XRD 分析結果顯示混合物的結晶性質隨著摻雜量而增加。表面微觀分析 FESEM 則顯示表面聚合物奈米複合材料的形態隨摻雜量的多寡而變化。純的 SnO_2 奈米顆粒形貌為球形尺寸約 100 nm，將 SnO_2 奈米顆粒加入 pure PVA-PVP 中會使得聚合物本體複合薄膜呈現粗糙表面形貌。AFM 研究顯示，在奈米複合薄膜的平均粗糙度隨摻雜劑濃度的變化而變化。

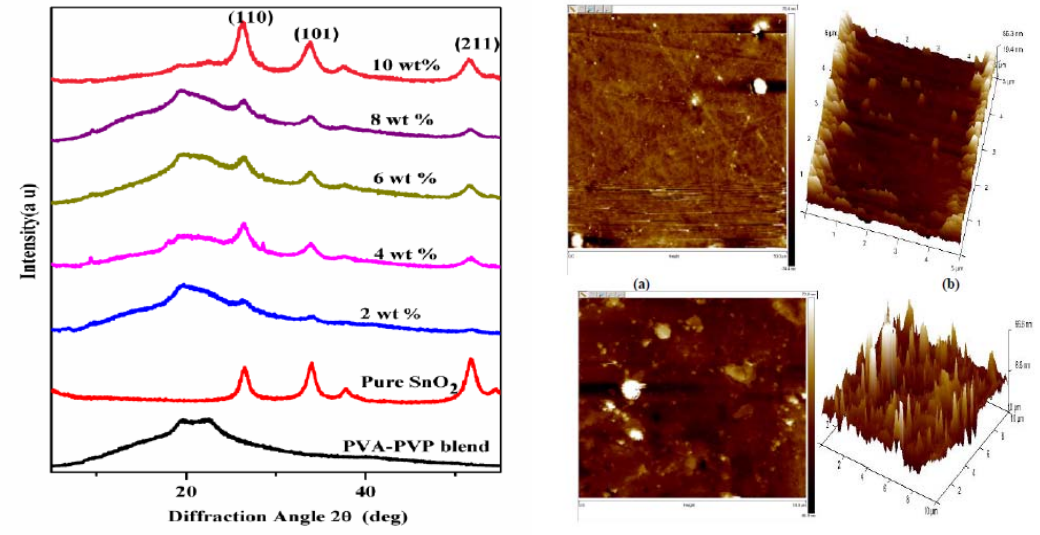

圖 14. PVA-PVP / SnO_2 奈米複合薄膜表面形貌分析 (From Sapporo Conference -ICMIM 2018 Abstract book)

(七) 日本大阪大學與甲南大學合作發表之論文：「Strong Hole Self-Doping in $LaMnO_3$ Thin Film on a-SiO_2 Substrate produced by Metal Organic Decomposition Method」，利用金屬有機共沉法(Metal Organic Decomposition Method, MOD)研究自摻雜 $LaMnO_3$（LMO）薄膜金屬研製與分析。隨著熱處理條件的不同，在 100 % O_2 氣氛中以 MOD 法製備 LMO 薄膜。由於在 LMO 結構中如遇製程環境中含有過量的 O^{2-}離子存在會導致自摻雜效應發生。製程溫度、時間與氣體氣氛皆是過量氧離子的形成原因。雖然 LMO 單晶是一種反鐵磁絕緣體，100 % O_2 氣氛中以 MOD 法製備 LMO 薄膜具有鐵磁金屬的特性。不同的熱處理條件下，分解有機物質為前驅物，樣品在空氣中在 400、500、600、700 或 800 °C 下預退火 10 分鐘。將前驅物以 900℃的 100 % O_2 氣氛中退火 1 小時可得結晶性，從電阻率的溫度依賴性的結果來看薄膜具有金屬 - 絕緣體轉變現象。在低溫下存在金屬相區域和高溫絕緣體相。磁性分析結果則發現在鐵磁相中存在鐵磁相低溫區域。研究人員以 MOD 法成功研製 LMO 薄

膜並且證明強空穴自摻雜 LMO 和鐵磁金屬的特性。

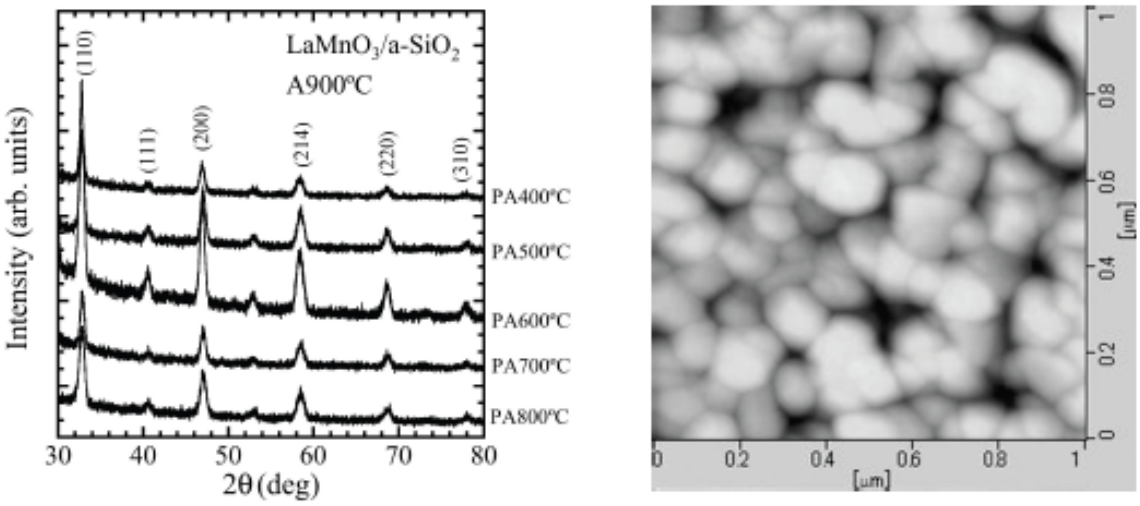

圖 15.LMO 薄膜 XRD 與表面形貌分析 (From Sapporo Conference -ICMIM 2018 Abstract book)

(八) 北海道大學應用化學系幅崎浩樹(Hiroki Habazaki)教授，針對質子傳輸型(Proton-conducting) SOFC 的研發成果簡要蒐集資訊如下。利用射頻磁控濺鍍法製備 $BaCe_{0.8}Y_{0.2}O_{3-\delta}$ 薄膜電解質（1 μm 厚度）於 $Pd_{1-x}Ag_x$ (x = 0,0.2 和 0.4）陽極之上，網印 LSCF 為陰極，研究 P-SOFC 在 600 ℃下的燃料電池性能。使用 $Pd_{0.8}Ag_{0.2}$ 陽極時較 $Pd_{0.6}Ag_{0.4}$ 具極佳之氫傳輸特性，最大功率密度在 600℃時達到 1.2 Wcm^{-2}，效能堪為陽極支撐質子傳輸型燃料電池（PCFCs）之冠。

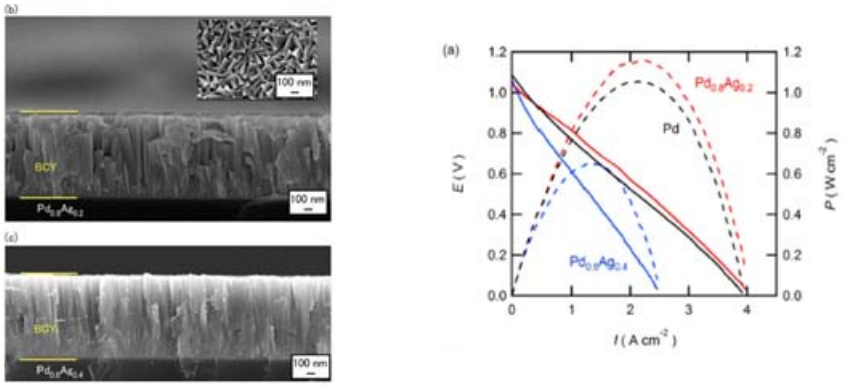

圖 16. 陽極支撐質子傳輸型燃料電池為結構與效能 (Y. Aoki, *et al.*, JES 164 (6) P.F577-F581 (2017))

(九) 典型的固態電解質裝置主要使用鉑電極材料和具氧化物離子傳導特性之釔安定氧化鋯（YSZ），傳統使用上其操作溫度至少高於 600°C，降低 SOFC 操作溫度是重要課題：開發高性能電極材料以及固態電解質材料、改進製程技術以提升介面間之有效反應形成。九州大學與三井金屬(Mitsui Kinzoku)有限公司合作研發，應用三井金屬專利開發的定向磷灰石型固態電解質材料（具有高氧化物離子傳導性），搭配由九州大學開發之具鈣鈦礦結構之氧化物電極（higher MIEC)材料和界面形成技術，成功地開發了一種能夠在中溫至低溫範圍內操作的固態電解質裝置。三井金屬開發的固態電解質材料具有高性能特性，其氧離子傳導率在 600°C 時超過 YSZ 的 10 倍，在 300°C 時則約為 YSZ 的 1,000 倍;而九州大學開發的電極材料在 400°C 及以下的溫度下顯示出高氧活性和良好的混合導性。製成的元件在 600°C 的溫度下施加 0.5V （DC）的電壓時顯示出 161mA / cm^2 的電流值。該電特性值比使用鉑電極和 YSZ 固態電解質的典型現有裝置高約 27 倍，證明這種裝置能夠在比現有裝置低約 200°C 的操作溫度範圍內操作。

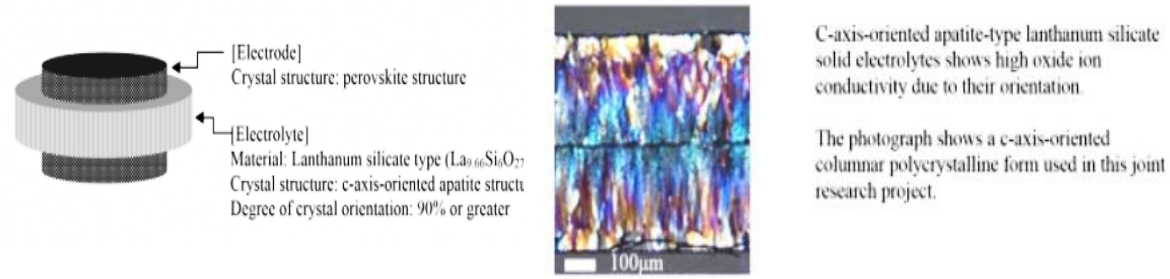

圖 17. 低溫型燃料電池開發之微結構

(*https://www.kyushu-u.ac.jp/en/researches/view/108*)

四、建議事項

本所為國家級研究單位，過去十多年於新及再生能源的研發領域投入許多心力與資源，其中 SOFC 之研發成效受到國際肯定，並積極參與國際上相關研討會。本次前往日本札幌市參加第 2 屆國際材料與智慧製造研討會(ICMIM 2018)國際研討會，以 SOFC-MEA 研發成果進行學術論文口頭發表，藉由此會議中氫能與燃料電池議題與國際上相關產學研專家學者討論燃料電池技術研發現況並建立研發資訊交流管道，以吸收國際上最新的 SOFC 發展資訊，藉此提升本所技術研發能量。無論於參與國際會議汲取新知，或論文發表彰顯研發成效，或與國際一流專家學者討論互動瞭解國際研究趨勢之層面，均感頗有收穫。幾點淺見建議如下：

（一） 國際材料與智慧製造研討會主要聚焦於材料與製造等領域，具備多元化的工程製造技術討論議題，參與會議及論文發表，對於促進國際學術交流、展現研發成果，以及提升技術水準與啟發研究創新，均有正面之效益。針對派員參加國際會議，建議除了持續維持本所在幾個主流 SOFC 相關國際研討會(如 ICACC、SOFC-XV 等)的參與度，對於其他材料製造分析等國際性綜合學術會議亦可依需求參加以提昇台灣之能見度並展現研發成果、開拓國際人脈。

（二） 本所長期投入 SOFC 燃料電池技術之開發，掌握關鍵技術已漸可與國際研發進展並駕，建議仍須積極建立並維繫與國內外之良好聲譽及連結關係，持續挹注資源，參與國際學術事務，與國際學術或研究機構，保持長期競合關係。

（三） 本所在 SOFC 之發展秉持 from powder to power 的研發主軸，唯目前已匯集了各方面整合型的研發成果並朝向技術產業化持續推動，除了材料研發之外，製造技術的強化與提升系統產品產業應用可行性時為重要議題。本次會議為材料與製造相關，建議本所相關研發除持續精進 SOFC 技術之外，亦值得投入資源於終端產品實務應用的推廣。

（四） 本所為國家實驗室級之研究機構，為保持研究水準及與國際趨勢契合，建議建立訪問學者及博士後研究員來所交流或研究之人力模式，吸引國內外一流科技人材，藉由競合之伙伴及工作氛圍，激盪腦力創新，提升本所研究水平及國際能見度。

附錄

Investigation on the Performance and Durability Behavior for the Anode-supported Solid Oxide Fuel Cell with Composite Cathodes

Tai-Nan Lin[1, a], Yang-Chuang Chang[1,b], Maw-Chwain Lee[1,c], Wei-Xin Kao[1,d]

[1]1000 Wenhua Rd. Jiaan Village, Longtan District, Taoyuan City 32546, Taiwan (ROC)

[a]tnlin@iner.gov.tw, [b]078701@cpc.com.tw, [c]mcleeretire@gmail.com, [d]wxkao@iner.gov.tw

Keywords: Anode-supported solid oxide fuel cell, yttria-stabilized zirconia, durability, electrochemical impedance spectroscopy

Abstract. The anode-supported solid oxide fuel cell (SOFC) comprises of NiO-8YSZ | 8YSZ | LSM-GDC | LSCF and the performance durability is executed for over 1000 hours. It shows low degradation phenomena under constant current operation during the complete testing period. The cell performance decreases with the decreasing of the temperature, and the maximum power densities are 408, 265, and 163 mW cm^{-2} at 800, 750, and 700 °C, respectively. According to the EIS analysis with the equivalent circuit model of five serial components, all resistances decrease with the testing time except the non-charge transfer resistance of the cathode. However all resistances increase with the decreasing of the temperature on the contrary. The ohmic resistance of the cell (R_O) dominates the cell performance under the whole durability test period as well as the operation temperature. In this study, the R_O is determined by the interfacial contact resistances, which occurred between the cell and the connecting components. The LSM-GDC | LSCF interfaces formed the discontinuous gap due to the weak attachment and external loading. The result of the activation energy analysis shows that the rate-determination step of the cell is existed in the

anode side between 700 and 800 °C. However, the cell performance is controlled from the domination of the R_O at 800 °C shift to the joint contributions of the R_O, anodic polarization (R_{AP}), and cathodic polarization (R_{CP}) at 700 °C.

Introduction

Solid oxide fuel cells (SOFCs) owning clean and efficient characteristics offer great promise as a next-generation energy converter. Many studies have been demonstrated that the SOFCs can achieve high electrical conversion efficiency more than 50 %. It is possible to improve the electrical efficiency to 70 % by combining with a gas turbine and to enhance the energy efficiency to 90 % by the equipments combined heat and power (CHP) [1-3]. Furthermore, due to the high-temperature operating environment, the SOFCs can run on a wide range of fuel sources such as methane, propane, LPG, natural gas, biogas, and even the coal. Therefore, the SOFCs have the ability to operate within both the current fossil-fuel infrastructure and the future hydrogen-fuel infrastructure.

For the commercial application of the SOFC technology, there are some importance requirements on the cost reduction, performance enhancement, and long-term stability. Generally, the lifetime requirement of the commercial product is more than 40,000 hours. Siemens Westinghouse has tested several tubular SOFC stacks / systems with power output from 0.4 to 220 KW, and the durability test is exceeding 20,000 hours [4]. However, the degradation of the cell performance is observed and there are complicated on the degradation mechanisms. Currently, many studies are devoted to proof the detail degradation mechanism and try to find out the solutions. The most typical degradation factors including the agglomeration of nickel, the change of nickel surface morphology, the change of the porosity, delamination, coking, contaminants poisoning, and so on [5-17]. In

addition, the operation conditions also result in the degradation of the cell performance, especially on the effect of the current density, thermal cycle and redox cycle [17-22].

For the compositions of the anode-supported SOFCs consisting of a zirconia-based electrolyte and the Ni cermet as the anode materials, these materials remain still considerable attraction because of the long-term reliability and cost factor. In this study, the anode-supported SOFC with a thin-film 8YSZ electrolyte has been successfully prepared by a sequential fabricating technique including tape casting, spin coating, and screen-printing. The structure of the cell comprises Ni-8YSZ (anode) | 8YSZ (electrolyte) | LSM-GDC (function layer) | LSCF (cathode), and the active area of the cell is about 13 cm^2. The durability test and electrochemical performance of the cell are executed with various constant current densities and operating temperatures. The cell performances are analyzed by the electrochemical impedance spectroscopy (EIS).

Experimental

Fabrication of the Single Cell. The anode-supported substrate was prepared by a tape casting process using a tape casting system (ECS Model CS-8) of laboratory model. Multiple green tape were laminated together in order to achieve an anode thickness of approximately 1 mm. The green anode substrate with an area of 5×5 cm^2 calcined at 1400 °C in air for 4 hours. The thin film electrolyte was manufactured onto the anode substrate by a spin coating process (Cee Model 200) and sintered at 1400 °C for 4 hours. The composite cathode layers were coated by the screen-printing (EKRA XPRT1) method. The cathode paste of the LSM-GDC (Fuel cell materials, FCM) was printed onto the YSZ electrolyte layer as the cathode functional layer (CFL) and sintered at 1150 °C for 3 hours. The LSCF paste (Fuel cell materials, FCM) was printed onto the CFL as the cathode current collector layer (CCCL) and

sintered at 1000 °C for 3 hours. Finally, the single cell with an active area of about 13 cm^2 was obtained.

Characterizations. The microstructure of the cross-section of the single cell was observed via a field emission scanning electron microscopy (FE-SEM, Hitachi, S-4800). The cell was tested in a cell test station consisting of alumina base with alumina flanges for gas distribution, and platinum and nickel meshes for the cathode and anode current collectors, respectively. Platinum wires were used as the current leads for cell voltage measurement. Air as an oxidant was available by the air supplier, and pure hydrogen as a fuel. The flow rates of the hydrogen fuel and the oxidant were 335 and 670 ml min^{-1}, respectively. The non-sealed type of the cell test was executed with a contact pressure of 25.4 KPa on the system of the SOFC-current collector [23]. The durability test of the cell with different constant current densities was operating for more than 1000 hours, and then the electrochemical performance of the cell was measured at 800, 750, and 700 °C. The measurements of the electrochemical impedance spectroscopy were conducted under open circuit operation using a Solartron 1260 frequency analyzer at the frequency range of 10 mHz to 105 Hz.

Results and Discussion

Microstructure of the Single Cell. Fig. 1 shows the typical SEM micrographs of the cross-section of the anode-support SOFC finished the performance test. The YSZ electrolyte layer is fully dense except the observation of a few closed pinholes, and the thickness of the YSZ electrolyte is about 6 μm. The thicknesses of the CFL and the CCCL are about 8 and 75 μm. The anode and the CFL with porous structures are firmly attached to the YSZ electrolyte. However, the long crevice is clearly observed between the CFL and the CCCL. It suggests that the structure between LSM-GDC and LSCF is a weaker attachment due to the lower

sintering temperature (chemical compatibility) and the difference of the thermal expansion coefficient (TEC) of the materials (mechanical compatibility). The weaker structure is easier ruined during the performance test of the cell because the requirement of the higher contact pressure results in the existence of the higher stress on the cell [23].

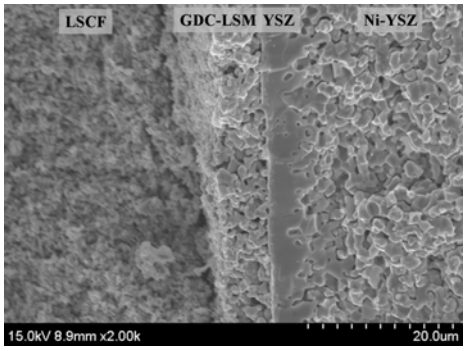

Fig. 1. The typical SEM micrographs of the cross-section of the anode-supported SOFC finished the performance test.

Performance and Durability Test of the Single Cell. The electrochemical performance test of the anode-supported SOFC was operated over 1000 hours. Cell voltage, temperature, current density and power density of the cell were recorded. Fig. 2 shows the electrochemical characterizations of the cell for the whole test process. The open-circuit voltage (OCV) of the cell is 1.041 V that indicates the structure of the YSZ electrolyte owns enough densification. The OCV deviation with the theoretical value (1.19 V at 800 °C) may come from the purity of gases and the water content under the non-sealed test environment [24]. Moreover, the performance evaluation of the cell mainly focuses on the output power and degradation rate of the cell. The degradation rate of the cell is defined as follow:

$\frac{V_i - V}{V_i}$.

(1)

where Vi is the initial cell voltage and V is the cell voltage at any time. The calculation of the degradation rate is must operate at a constant current density. Table 1 lists the characteristics and degradation rates of the cell under different operation conditions. These results show that the higher constant current density can serve more output power, and no degradation occurs under different constant current densities, even operated more than 800 hours at constant current density of 400 $mAcm^{-2}$. The kinetic of the cell degradation in the operation condition of the steady state mode often occurs in three phases [17]. The first phase is ascribed to the reorganization of the electrode microstructure, which can lead the performance increasing or decreasing. The second phase shows a continuous degradation of the cell performance, and the variation of the cell voltage is often used as the degradation rate of the cell. The third phase shows the performance decreases rapidly. The most studies report that the change of electrode microstructure is occurred during the cell test, such as the agglomeration of nickel, the change of nickel morphology, the breakdown of the ceramic/nickel network, the change of the porosity, the separation of phases, and so on [5-6, 25]. However, these

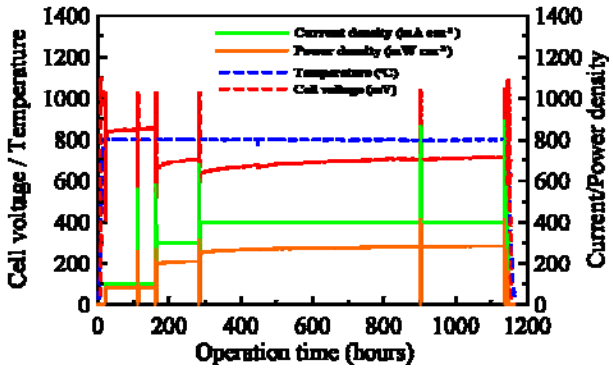

Fig. 2 The electrochemical characterizations of the cell for the whole test process.

reports present the degradation of the cell performance and it cannot satisfy our results. According to our previous study [26], the breeding mechanism of the nano-scale nickel catalyst on the anode side results in the cell voltage increases slowly with time at a constant current density. The same phenomenon is observed in this study, and this phenomenon is still existed as the constant current density increases systematically. Therefore, it suggests that the whole durability test without any degradation occurs in the first phase, and the change of the electrode microstructure includes at least the breeding of nickel catalyst that gains the cell performance.

Table 1 The characteristics and degradation rates of the cell under different operation conditions

Measured Point	Time (hrs)	Temperature (°C)	Fixed I (mA cm^{-2})	V (mV)	P_{output} (mW cm^{-2})	Degradation rate (%)
P1	21	800	100	805	80	—
P2	113	800	100	849	85	0
P3	161	800	100	854	85	0
P4	164	800	300	640	193	—
P5	282	800	300	703	211	0
P6	285	800	400	625	251	—
P7	902	800	400	705	282	0
P8	1138	800	400	716	286	0

Fig. 3 shows the I-V-P curves of the cell at 800 °C under different operation conditions. This result presents that the cell performance increases slightly with time at a constant current density and increases obviously with the increasing of the constant current density.

The maximum power densities of the measured points with the increasing of the operation time are 260, 271, 315, 395, and 408 $mWcm^{-2}$, respectively. Fig. 4 shows the I-V-P curves of the cell at different temperatures. The cell performance decreases dramatically with the decreasing of the temperature, and the maximum power densities are 408, 265, and 163 $mWcm^{-2}$ at 800, 750, and 700 °C, respectively. The electrochemical performance of the cell decreases about 60 % as the temperature decrease from 800 to 700 °C. To examine the difference of the cell performance under different operation conditions, the more detail electrochemical impedance analysis is carried out.

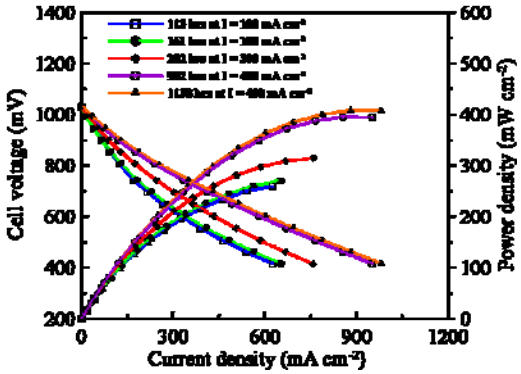

Fig. 3 The *I-V* and *I-P* curves of the cell at 800 °C under different operation conditions.

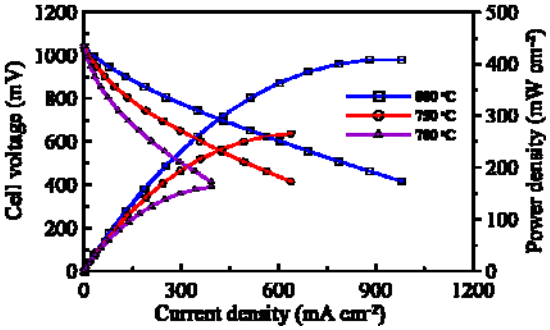

Fig. 4 The *I-V* and *I-P* curves of the cell at 700, 750, and 800 °C.

EIS Analysis. In the past years, it is well know that the electrode polarization of the cell is using the simulation model of the equivalent circuit with three serial components which indicate the ohmic resistance of the cell, the charge transfer polarization and the non-charge transfer polarization at the high and low frequency domains, respectively [27-29]. That means the contributions of the cathode and anode are simultaneously existed in the individual arcs. Hence, this information provides the clew for the frequency selection used for the model simulation. In order to distinguish and identify the contribution of each element resistance, the equivalent circuit model of the five serial components [30-31] was employed in this study and the impedance spectrum was fitted using the ZView2 program. The criteria of the accuracy between the experimental data and the simulating result which combines the five variables is defined by that the value of the Gaussian Distribution of Activation Energy Accuracy (GDAE accuracy) is set at 2. Fig. 5 presents the Nyquist impedance spectrum of the cell at the measured point of P3. The L_0 is the inductance, which is attributed to the Pt probes or the high-frequency phase shift of electrochemical equipment. The CPEs represent the constant phase elements of the arcs [32]. The intercept of the high frequency and the real axis represents the ohmic resistance of the cell (R_O). This resistance is ascribed to the sum of the ohmic resistance of the cell comprising the anode, cathode, and electrolyte, and some contact resistances of the interfaces between the cell and the connecting components, such as the current collection and lead wires. The sequential resistances (R_1, R_2, R_3, R_4) are depicted the four arcs from high frequency to low frequency. R_1 and R_2 are used to describe the charge transfer polarizations in the cathode and anode, respectively. Those are related to the transport of the charged species in the electrodes, including the electron, the oxygen and hydrogen ions, and the interface transport of the oxygen ion between the electrolyte and the cathode/anode. R_3 and R_4 represent the

non-charge transfer polarizations, including gas diffusion and reaction, in the cathode and anode, respectively.

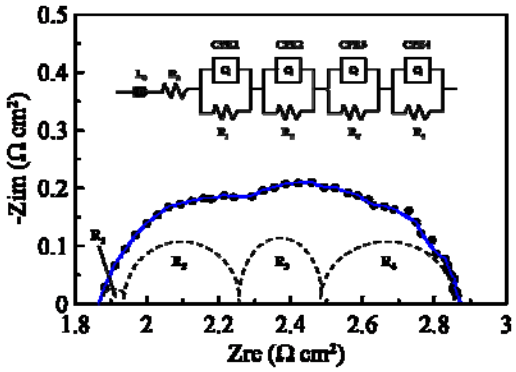

Fig. 5 The Nyquist impedance spectrum of the cell at the measured point of P3. Measured date (symbols), fitted spectrum (solid line), and fitted spectrum depicted as the four arcs (dotted line).

The Nyquist impedance spectra of the cell under different operation conditions are shown in Fig. 6. The fitting lines are well consistent with the measured data, and the fitting parameters of the EIS analysis of the cell under different operation times and temperatures are plotted in Fig. 7. From the result of the Fig. 7 (a), the value of R_3 is independent of time and current density. However, the value of R_1 is obviously decreasing from 0.386 Ωcm^2 at P2 point to 0.199 Ωcm^2 at P8 point, particularly at the early period (from P2 to P3). Some studies have observed the cathodic polarization loss and indicate that this effect is attributed to the change of the three phase boundary (TPB) and / or the microstructure, the remove of the surface passive layer associated with the segregated phase of the Sr and / or La species on the surface of LSM, the partial reduction of the cathode, and the formation of the oxygen vacancies [33-36]. For the composite cathode layer of LSM-GDC / LSCF in this

study, the cathodic activation process is mainly contributed to the decreasing of the charge transfer resistance (R_1), such as the enhancement of the oxygen vacancy, the remove of impurity phases, and / or the current path change depending on the constant current density [37]. Furthermore, the values of R_2 and R_4 decrease with the increasing of the operation time. The slight change of the R_2 value may be caused by the current path change of the anode as the change of constant current density [38]. According our previous study, the activation period of the anode is about operation time of 200-300 hours. In this activation period, the nano-size Ni catalyst is breeding quickly and that improves the catalysis of the anode. It interprets that the R_4 value decreases rapidly in the early stage of the cell test. After activation process, the R_4 value decreases slowly that may be caused by the change of the anode microstructure. In addition, it is noteworthy that the $R_1 > R_2$ which indicates that the charge transfer resistance of the anode is smaller than that of the cathode. That is reasonable because the discontinuous gap exists between LSM-GDC and LSCF from the observation of the SEM image. However, the result of $R_4 > R_3$ indicates that the non-charge transfer resistance of the anode is higher than that of the cathode. That is inconsistent with the literatures that propose that the electrode polarization is mainly attributed to the reduction reaction of the oxygen in the cathode due to the poor activity of the catalyst. It deduces reasonably that the porosity of the anode is not enough resulting in the increasing of the anodic polarization.

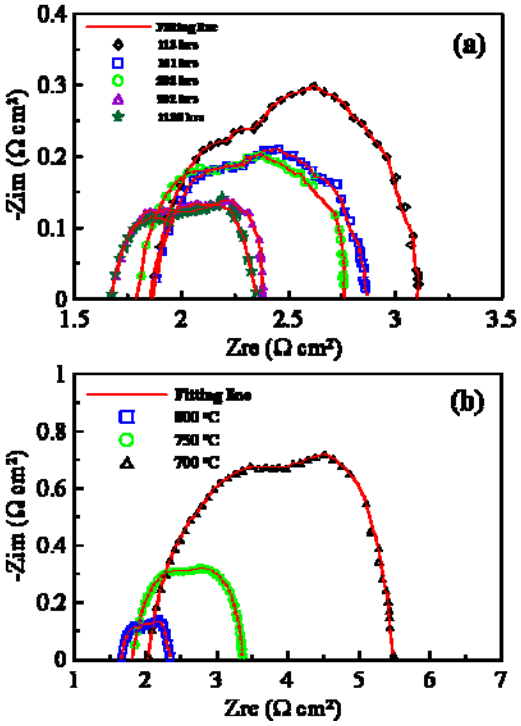

Fig. 6. The Nyquist impedance spectra of the cell under different operation conditions: (a) different operation times, and (b) different operation temperatures. Measured date (symbols), and fitted spectrum (solid line).

From the result of the Fig. 7 (b), all variables (R_1, R_2, R_3, R_4) are increasing with the decreasing of the temperature. As the temperature decreases, the catalyst activity of the anode and cathode is decreasing and the transfer of the oxygen ion in the cathode, electrolyte, and anode is decreasing rapidly. Moreover, the R_1 and R_4 are higher relationship with the temperature in this study. It implies that the cell performance is strongly affected by the mechanical structure of the cell, such as the TEC mismatch of the materials, and the poor porosity of the anode for the intermediate-temperature operation.

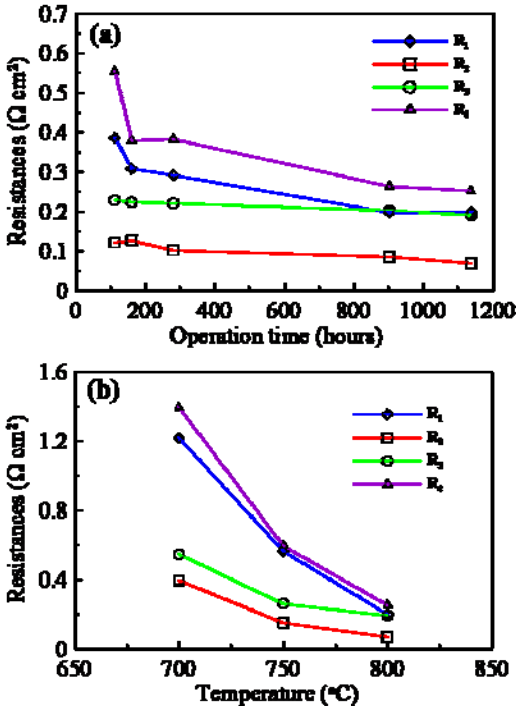

Fig. 7 (a) The relationship of individual resistance (R_1, R_2, R_3, R_4) and the operation time, and (b) the relationship of individual resistance and the operation temperature.

To understand the individual contribution of each element of the cell, the resistances of the anode, cathode, and electrolyte are presented. According to the definition of each resistance, the anodic polarization (R_{AP}) is the sum of the R_2 and R_4, and the cathodic polarization (R_{CP}) is the sum of the R_1 and R_3. The total resistance of the cell (R_T) is the summed value of the R_{AP}, R_{CP}, and R_O. The relationships of those resistances versus the time and temperature are shown in Fig. 8. From the result of the Fig. 8 (a), it is obviously observed that the contributions of the anodic and cathodic polarization are considerable equal, and the ohmic resistance of the cell (R_O) is dominated the cell performance during the durability test. Generally, the ohmic resistance is mainly regard as the contribution of the electrolyte resistance (R_E), and the estimated resistance expression of the 8YSZ electrolyte is shown as follow:

$$\rho_E = 0.00294 e^{\left(10350/T_{cell}\right)}.$$

(2)

In this study, the calculated value of the R_E is 0.032 Ωcm^2 at 800 °C that is much lower than the R_O value obtained from the EIS analysis. Leone *et al*. reported the similar result that the ratio of the R_E to the R_O is about 15 % from 740 to 840 °C [39]. This result is suggesting that the ohmic resistance is dominated by the interfacial contact resistances, which are occurred between the cell and the connecting components and between the components inside the cell if the delamination/crack is formed. Moreover, from the result of the Fig. 8 (b), the anodic and cathodic polarizations fairly increase simultaneous quickly with the decreasing of the temperature. The cell performance is controlled from the domination of the ohmic resistance at 800 °C shift to the joint contributions of the R_O, R_{AP}, and R_{CP} at 700 °C.

Fig. 9 shows the Arrhenius plots of the resistances of the cell. The resistances (R_O, R_{AP}, R_{CP}, R_T) are well described by an Arrhenius equation from 700 to 800 °C. Although the activation energy (Ea) has not been well clearly understood yet, it provides a powerful clew to analyze the consequence of the energy barrier for each component of the cell. The anodic polarization of the cell shows the maximum value of the activation energy (149 KJmol^{-1}) which indicates that the rate-determination step of the cell is existed in the anode side. Therefore, the poor electrochemical performance of the cell is resulted from the characteristics of the anode, such as the porosity, TPB length, electro-catalyst, and so on. Among these characteristics, the anodic porosity might be a key factor in this study. The low porosity of the anode inhibits gas diffusion, especially for the water product removal out of the pore structure. Poor water diffusion is not favorable for hydrogen supply and

further diminishes the reaction conversion. This effect is obviously observed at the lower operating temperature because the reaction zone is extended far away from the interface of the electrolyte due to the poor anodic porosity and the oxygen-ion transfer is slow in the YSZ network of the anode cermet. In addition, the activation energy of the ohmic resistance is the smallest and close to zero, that indicates the R_O is slightly dependent on the temperature. That is reasonable because the R_O is dominated by the interfacial contact resistances, not the ohmic resistance of the electrolyte.

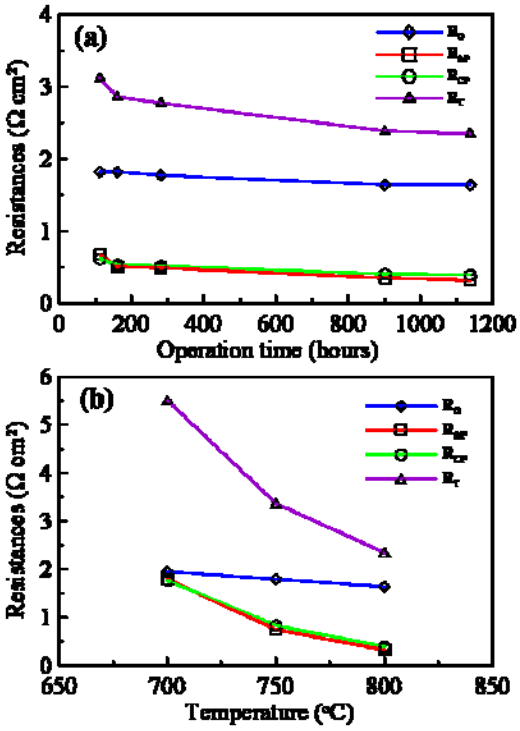

Fig. 8 (a) The relationship of the resistances (R_O, R_{AP}, R_{CP}, R_T) and the operation time, and (b) the relationship of the resistances and the operation temperature.

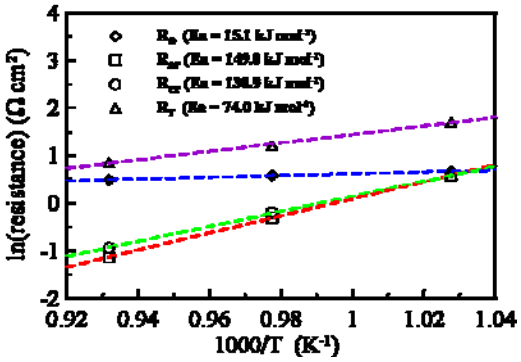

Fig. 9. The Arrhenius plots of the resistances (R_O, R_{AP}, R_{CP}, R_T) for the anode- supported SOFC.

Conclusions

The durability test on the anode-supported SOFC comprising Ni-8YSZ | 8YSZ | LSM-GDC | LSCF was investigated over 1000 hours. From the performance test of the cell, no degradation occurs under different constant current densities during the whole durability test. The improvement performance with time is caused by the change of the electrode microstructure, and one of the mechanisms is the phenomenon of the nickel catalyst breeding. Moreover, the cell performance decreases dramatically with the decreasing of the temperature, and the maximum power densities are 408, 265, and 163 $mWcm^{-2}$ at 800, 750, and 700 °C, respectively. The EIS analysis which using the equivalent circuit model with five serial components is applied in this study, and the fitting results of the EIS analysis offer some significant information to understand the contribution of the individual resistance of the cell. First, all resistances are decreasing with time except the non-charge transfer resistance of the cathode (R_3) that indicates that the catalytic activity of the cathode is not change with time at 800 °C. Second, the ohmic resistance of the cell (R_O) is dominated the cell performance under the whole durability test and the effect of the temperature. In this study, the R_O is dominated by the interfacial contact resistances, which are occurred between the cell and the connecting

components and between LSM-GDC and LSCF that formed the discontinuous gap due to the weaker attachment and external loading. Third, all resistances increase with the decreasing of the temperature, especially in the charge transfer resistance of the cathode (R_1) and the non-charge transfer resistance of the anode (R_4). The contribution of the R_1 is mainly ascribed to the crack formation on the composite cathode, and the contribution of the R_4 is mainly caused by the poor porosity of the anode. It suggests that the anodic porosity and mechanical structure of the cell influence strongly the cell performance. Finally, the result of the activation energy analysis shows that the rate-determination step of the cell is existed in the anode side (R_{AP}) between 700 and 800 °C. However, the cell performance is controlled from the domination of the R_O at 800 °C shift to the joint contributions of the R_O, R_{AP}, and R_{CP} at 700 °C. The as-prepared cells exhibit certain output power performance and durability. However to shorten the cell startup time as well as the activation process will be the critical concern before real application in cell products.

Acknowledgment

Drs. Tai-Nan Lin and Yang-Chuang Chang thanks Drs. Chun-Hsiu. Wang, Rung-Je Yang, Mrs. Jen-Cheng Chang, Ling-Song Lee, Hong-Yi Kuo, Chun-Yen Yeh, for the cell fabrication experimental supports as well as the technical discussions on this work.

References

[1] M. Yokoo, Y. Tabata, Y. Yoshida, H. Orui, K. Hayashi, Y. Nozaki, K. Nozawa, H. Arai: J. Power Sources Vol. 184 (2008), p. 84

[2] B. Rietveld: ECS Transactions Vol. 7 (2007) p. 17

[3] X. Zhang, J. Li, G. Li, Z. Feng: J. Power Sources Vol. 163 (2006) p. 523

[4] S.C. Singhal, K. Kendall, *High Temperature Solid Oxide Fuel Cells: Fundamentals, Design and Applications* (Elsevier Ltd., Oxford, 2004)

[5] A. Hagen, R. Barfod, P.V. Hendriksen, Y.L. Liu, S. Ramousse: J. Electrochem. Soc. Vol. 153 (2006) P. A1165

[6] D. Simwonis, F. Tietz, D. Stöver: Solid State Ionics Vol. 132 (2000) p. 241

[7] T. Suzuki, Z. Hasan, Y. Funahashi, T. Yamaguchi, Y. Fujishiro, M. Awano: Science Vol. 325 (2009) p. 852

[8] M.D. Gross, J.M. Vohs, R.J. Gorte: J. Mater. Chem. Vol. 17 (2007) p. 3071

[9] Y.H. Huang, R.I. Dass, J.C. Denyszyn, J.B. Goodenough: J. Electrochem. Soc. Vol. 153 (2006) p. A1266

[10] N.M. Tikekar, T.J. Armstrong, A.V. Virkar: J. Electrochem. Soc. Vol. 153 (2006) p. A654

[11] M. Mogensen, K.V. Jensen: Solid State Ionics Vol. 150 (2002) p. 123

[12] L. Yang, S. Wang, K. Blinn, M. Liu, Z. Liu, Z. Cheng, M. Liu: Science Vol. 326 (2009) p. 126

[13] M. Flytzani-Stephanopoulos, M. Sakbodin, Z. Wang: Science Vol. 312 (2006) p. 1508

[14] Y.L. Liu, C. Jiao: Solid State Ionics Vol. 176 (2005) p. 435

[15] Y. Matsuzaki, I. Yasuda: J. Electrochem. Soc. Vol. 148 (2001) p. A126

[16] A. Mai, M. Becker, W. Assenmacher, F. Tietz, D. Hathiramani, E. Ivers-Tiffée, D. Stöver, W. Mader: Solid State Ionics Vol. 177 (2006) p. 1965

[17] H. Yokokawa, H. Tu, B. Iwanschitz, A. Maic: J. Power Sources Vol. 182 (2008) p. 400

[18] T. Kawada, N. Sakai, H. Yokokawa, M. Dokiya, M. Mori, T. Iwata: J. Electrochem. Soc. Vol. 137 (1990) p. 3042

[19] H. Uchida, M.Yoshida, M.Watanabe: J. Electrochem. Soc. Vol. 146 (1999) p. 1

[20] D. Sarantaridis, A. Atkinson: Fuel Cells Vol. 7 (2007) p. 246

[21] D.Waldbillig, A.Wood, D.G. Ivey: J. Power Sources Vol. 145 (2005) p. 206

[22] W. Bujalski, C.M. Dikwal, K. Kendall: J. Power Sources Vol. 171 (2007) p. 96

[23] W.X. Kao, M.C. Lee, Y.C. Chang, T.N. Lin, C.H. Wang, J.C. Chang: J. Power Sources Vol. 195 (2010) p. 6468

[24] H.Y. Jung, S.H. Choi, H. Kim, J.W. Son, J. Kim, H.W. Lee, J.H. Kim: J. Power Sources Vol. 159 (2006) p. 478

[25] T. Iwata: J. Electrochem. Soc. Vol. 153 (1996) p. 1521

[26] C.H. Wang, M.C. Lee, T.J. Huang, Y.C. Chang, W.X. Kao, T.N. Lin: Electrochem. Comm. Vol. 11 (2009) p. 1381

[27] Y.J. Leng, S.H. Chan, K.A. Khor, S.P. Jiang: Int. J. Hydrogen Energy Vol. 29 (2004) p. 1025

[28] S. Li, Z. Lu, N. Ai, K. Chen, W. Su: J. Power Sources Vol. 165 (2007) p. 97

[29] W. X. Kao, M. C. Lee, T. N. Lin, C. H. Wang, Y. C. Chang: J. Power Sources Vol. 195 (2010) p. 2220

[30] R. Barfod, M. Mogensen, T. Klemensø, Anke Hagen, Y.L. Liu, P.V. Hendriksen: J. Electrochem. Soc. Vol. 154 (2007) p. B371

[31] S. Le, K. N. Sun, N. Zhang, X. Zhu, H. Sun, Y.X. Yuan, X. Zhou: J. Power Sources Vol. 195 (2010) p. 2644

[32] K.A. Khor, S.H. Chan: J. Power Sources Vol. 123 (2003) p. 17

[33] S.P. Jiang, J.P. Love: Solid State Ionics Vol. 138 (2001) p. 183

[34] S.P. Jiang, J.G. Love, J.P. Zhang, M. Hoang, Y. Ramprakash, A.E. Hughes, S.P.S. Badwal: Solid State Ionics Vol. 121 (1999) p. 1

[35] F.H. Van Heuveln, H.J.M. Bouwmeester: J. Electrochem. Soc. Vol. 144 (1997) p. 134

[36] H.Y. Lee, W.S. Cho, S.M. Oh, H.D. Wiemhöfer, W. Göpel: J. Electrochem. Soc. Vol. 142 (1995) p. 2659

[37] M. Suzuki, et al., In Proceedings of the 2nd IFCC (International Fuel Cell Conference), Kobe, Japan NEDO, 1966.

[38] H. Uchida, M. Yoshida, M. Watanabe: J. Electrochem. Soc. Vol. 146 (1999) p. 1

[39] P. Leone, M. Santarelli, P. Asinari, M. Calí, R. Borchiellini: J. Power Sources Vol. 177 (2008) p. 111